Calibration of the Hobson&Rogers model: empirical tests.

Paolo Foschi and Andrea Pascucci
Dipartimento di Matematica, Università di Bologna *

Abstract

The path-dependent volatility model by Hobson and Rogers is considered. It is known that this model can potentially reproduce the observed smile and skew patterns of different directions, while preserving the completeness of the market. In order to quantitatively investigate the pricing performance of the model a calibration procedure is here derived. Numerical results based on S&P500 option prices give evidence of the effectiveness of the model.

1 Introduction

This paper aims to propose a flexible calibration procedure of the Hobson and Rogers (HR) model [18] and to investigate the performance by testing it on a set of S&P500 option data. Among non-constant volatility models in complete markets, the HR model seems to be one of the more appealing. In this model the volatility σ is supposed to depend on the trend of the underlying asset, defined as the difference of the spot price S and a weighted average of past prices. This feature seems to be more realistic and natural compared with the usual assumption $\sigma = \sigma(t, S)$ of the widespread level-dependent models: for instance, it is known that the volatility increases after a market reversal and this is difficultly captured by a model which only takes into account of the present price of the underlying.

In the HR setting no exogenous source of risk is added so that the market completeness is preserved and the standard arbitrage pricing theory applies. Moreover this model is potentially capable to reproduce the observed smile and volatility term structure patterns. For practical purposes, the HR model allows to price exotic derivatives consistently with vanilla options which are commonly traded on markets, keeping into account of smiles and skews. Despite of its fine features, so far little has been done in the empirical analysis of the model. Figà-Talamanca and Guerra [14] examined the problem of the estimation of the parameters of the model and a generalization was proposed by Hubalek, Teichmann and Tompkins [19]. The HR model has also been considered by Hallulli and Vargiolu [3] and an extension to the framework of term-structure modeling was given by Chiarella and Kwon [5].

In order to present our results, we first recall the main features of (a simplified version of) the HR model. In a Wiener space with one-dimensional Brownian motion (W_t), we denote by

*Piazza di Porta S. Donato 5, 40126 Bologna (Italy). E-mail: foschip@csr.unibo.it, pascucci@dm.unibo.it

S_t the stock price and by D_t the deviation of prices from the trend, defined by

$$D_t = Z_t - \int_0^{+\infty} \lambda e^{-\lambda\tau} Z_{t-\tau} d\tau, \qquad \lambda > 0, \tag{1.1}$$

where $Z_t = \log(e^{-rt}S_t)$ is the discounted log-price. In (1.1), the parameter λ amounts to the rate at which past prices are weighted. Hobson and Rogers assume that S_t is an Itô process, solution to the stochastic differential equation

$$dS_t = \mu(D_t)S_t dt + \sigma(D_t)S_t dW_t. \tag{1.2}$$

In (1.2), μ and $\sigma > 0$ are deterministic functions satisfying usual hypotheses in order to guarantee that the system of SDEs (1.1)-(1.2) is uniquely solvable. Finally, we denote by U_{T-t} the price at time t of an European contingent claim with exercise date T.

A key feature of the model is that the process (S_t, D_t) is Markovian (cf. Lemma 3.1 in [18]). Then if we consider the time t, the price S_t and the mean $M_t = \log(e^{rt}S_t) - D_t$ as state variables and assume that

$$U_{T-t} = e^{-rt} f(S_t, M_t, t) \tag{1.3}$$

for some smooth function f, then f satisfies the PDE in $\mathbb{R}^3$:

$$\frac{\sigma^2(Z-M)S^2}{2}\,\partial_{SS} f + rS\partial_S f + \lambda(\log S + rt - M)\partial_M f - \partial_t f = 0. \tag{1.4}$$

As in the Black&Scholes framework, the drift term in (1.2) does not enter in the valuation PDE while a key role is played by the volatility function σ which is an input of the model and has to be estimated in order to fit market observations. Aiming to motivate the model, Hobson and Rogers consider in [18] a volatility function of the form

$$\sigma(D) = \min\left\{\eta\sqrt{1+\varepsilon D^2}, N\right\} \tag{1.5}$$

for some large constant N and positive parameters ε, η: then they show that the model can indeed exhibit smiles and skews of different directions. In this note we aim to select σ without imposing a priori assumptions on its shape but simply calibrating it to market prices of plain vanilla options. In order to maintain the approach as much flexible as possible, we assume that σ is approximated in a space of piecewise cubic Hermite polynomial (see [16]).

At first glance, this calibration problem is similar to that in the framework of Dupire's implied diffusion theory [13] where the asset price S_t solves a SDE of the form

$$dS_t = \mu(t, S_t)dt + \sigma(t, S_t)dW_t.$$

Dupire model is consistent with the market implied volatility smile provided that the function σ is *continuously* calibrated to the market by the Dupire's local volatility formula. Several major derivatives houses have this model implemented.

On the other hand the HR model seems to have two main advantages. Firstly, in a path-dependent model the volatility incorporates information on the past and, in particular, on the preceding behavior of investors. Then, in some sense, the model "knows" how investors behave

in different market circumstances and can also keep into account of the (positive or negative) trend of the asset. For this reason it seems that the HR model does not need to be continuously re-calibrated: for practical use, in many cases it should be sufficiently reliable as soon as it is calibrated once a week.

Secondly, due to some invariance property of (1.4), a simple change of variables allows to evaluate all European option prices corresponding to different strikes and different time-to-maturities in a single run (cf. Remark 2.1). This considerably speed up the calibration procedure by PDEs' techniques. Actually the PDE approach also has the natural advantage of allowing to compute the derivatives with respect to the parameters (or Greeks) of the solution which will be useful in the procedure.

The paper is organized as follows. In Section 1 we recall some numerical result for the HR model in the framework of PDEs of Kolmogorov type. Then, in Section 2 the inverse problem arising in the calibration is stated as a simple nonlinear least squares problem. In the last part of the paper, the results of the calibration are tested on a set of S&P500 index options prices and experimental results regarding the fitting of the model to observed prices are presented.

2 Numerical preliminaries

In this section we briefly recall the numerical results in [7, 8] for the Hobson&Rogers. In case of an European call option with strike K, equation (1.4) is coupled with the following initial conditions

$$f(S, M, 0) = (S - K)^+. \tag{2.1}$$

We rewrite equation (1.4) as

$$\mathcal{L}u \equiv a(\partial_{xx}u - \partial_x u) + (x - y)\partial_y u - \partial_t u = 0, \tag{2.2}$$

where $u = u(x, y, t)$ is determined by the transformation

$$f(S, M, t) = Ku\left(\log(S/K) + rt, M - log(K), \lambda t\right) \tag{2.3}$$

and it has been set

$$a(x, y) = \frac{\sigma^2(x - y)}{2\lambda}. \tag{2.4}$$

By this change of variables, problem (1.4)-(2.1) is equivalent to the Cauchy problem for (2.2) in the strip $\mathbb{R}^2 \times [0, \lambda T]$ with initial condition

$$u(x, y, 0) = (e^x - 1)^+ \qquad \text{for } (x, y) \in \mathbb{R}^2. \tag{2.5}$$

Remark 2.1. *Problem* (2.2)-(2.5) *is independent of* K. *Then, by formula* (2.3), *we obtain option prices corresponding to different strikes by solving a unique PDE.*

Due to the additional state variable M on which the option price depends, equation (2.2) is of degenerate type since the quadratic form associated to the second order part of $\mathcal{L}$ is singular. However (2.2) belongs to the noteworthy subclass of Hörmander PDEs today called of Kolmogorov or Ornstein-Uhlenbeck type. For this class a very satisfactory theory has been

developed and many sharp analytical results are available even under weak regularity assumptions (see [20] for an exhaustive survey on this topic). In particular, in [10] it is proved that if the coefficient a is a bounded and uniformly positive Hölder continuous function then problem (2.2)-(2.5) has a unique classical solution u and sharp estimates for u and its derivatives are provided.

2.1 Finite difference schemes of Kolmogorov type for the pricing PDE

The natural framework for the study of the properties of equation (2.2) is the analysis on Lie groups (cf. [20]). Also in the numerical approximation the best results are obtained in a non-Euclidean setting: for instance, it is known that the differential operators ∂_x and

$$Yu = (x-y)\partial_y u - \partial_t u \tag{2.6}$$

are the main (in some intrinsic sense) directional derivatives of the degenerate equation (2.2). Therefore, in the numerical solution of the option pricing equation by finite-difference methods, it is natural and more efficient to approximate the main directional derivatives rather than the usual Euclidean ones. In this section we recall some of the results of [8] about the so-called finite difference schemes of Kolmogorov type. The main features of these schemes are the following:

i) in the discretization of the PDE in a finite region, *no boundary conditions on the y-variable are required.* This is a significant advantage since there are no obvious financial motivations for imposing conditions on the option price $f(S, M, t)$ for some fixed M;

ii) solving the scheme only involves the inversion of a *tri-diagonal* matrix which leads to a fast and easy implementation.

We consider the uniform grid

$$G = \{(i\Delta_x, j\Delta_y, n\Delta_t) \ \mid \ i, j, n \in \mathbb{Z}, \ n \geq 0\}, \tag{2.7}$$

and approximate as usual the derivatives $\partial_x u$ and $\partial_{xx} u$ by the centered differences and the three-point schemes, respectively:

$$\partial_x u(x,y,t) \quad \sim \quad D_{\Delta_x} u(x,y,t) = \frac{u(x+\Delta_x, y, t) - u(x-\Delta_x, y, t)}{2\Delta_x}, \tag{2.8}$$

and

$$\partial_{xx} u(x,y,t) \quad \sim \quad D^2_{\Delta_x} u(x,y,t) = \frac{u(x+\Delta_x, y, t) - 2u(x,y,t) + u(x-\Delta_x, y, t)}{\Delta_x^2}, \tag{2.9}$$

Thus, the approximation

$$\begin{aligned} \partial_{xx} u(x,y,t) - \partial_x u(x,y,t) \quad \sim \quad & D^2_{\Delta_x} u(x,y,t) - D_{\Delta_x} u(x,y,t) \\ & = d_1 u(x-\Delta_x, y, t) + d_2 u(x,y,t) + d_3 u(x+\Delta_x, y, t), \end{aligned} \tag{2.10}$$

with $d_1 = 1/\Delta_x^2 + 1/(2\Delta_x)$, $d_2 = -2/\Delta_x^2$ and $d_3 = 1/\Delta_x^2 - 1/(2\Delta_x)$, is of order Δ_x^2.

The second main derivative Y is approximated either by

$$Yu(x,y,t) \sim Y^+_{\Delta_t}u(x,y,t) = \frac{\widetilde{u}(x,y,t) - \widetilde{u}(x,y-(x-y)\Delta_t,t+\Delta_t)}{\Delta_t}, \tag{2.11}$$

or by

$$Yu(x,y,t) \sim Y^-_{\Delta_t}u(x,y,t) = \frac{\widetilde{u}(x,y+(x-y)\Delta_t,t-\Delta_t) - \widetilde{u}(x,y,t)}{\Delta_t}, \tag{2.12}$$

where $\widetilde{u}(x,y,t)$ denotes the linear interpolation of u at the point (x,y,t) based on the two nearest grid points. Specifically,

$$\widetilde{u}(x,y,t) = (1-\gamma)u(x,\widetilde{y},t) + \gamma u(x,\widetilde{y}+\Delta_y,t), \tag{2.13}$$

where $\gamma = (y-\widetilde{y})/\Delta_y$ and $\widetilde{y} = [y/\Delta_y]\,\Delta_y$ denoting by $[\cdot]$ the integer part. Since $\widetilde{u}(x,y,t)$ approximates $u(x,y,t)$ with an error of the order of Δ_y, then the approximations (2.11) and (2.12) are of the order of $\Delta_t + \Delta_y$. We remark that interpolation (2.13) is necessary because (x,y,t) and $(x,y-(x-y)\Delta_t,t-\Delta_t)$ cannot both belong to the same uniform grid. In [7] a different change of variables has been proposed in place of (2.3). That approach allowed for both the points to belong to the grid, but at the cost of imposing the grid size condition $\Delta_y = \Delta_x\Delta_t$.

The discrete operators $\mathcal{L}^+_G$ and $\mathcal{L}^-_G$ are defined by

$$\mathcal{L}^\pm_G u = a(D^2_{\Delta_x}u - D_{\Delta_x}u) + Y^\pm_{\Delta_x}u \tag{2.14}$$

and approximate $\mathcal{L}$ in the sense that

$$\|\mathcal{L}u - \mathcal{L}^\pm_G u\|_{L^\infty} \le C\left(\Delta_x^2 + \Delta_t + \frac{\Delta_y^2}{\Delta_t}\right), \tag{2.15}$$

for some positive constant C depending on the L^∞-norms of a, $\partial_{xxx}u$, $\partial_y u$, $\partial^4_x u$, Y^2u, $\partial_{xx}Yu$, and $\partial_{xxy}u$ on the domain.

Hereafter, we refer to $\mathcal{L}^+_G$ and $\mathcal{L}^-_G$ respectively as explicit and implicit schemes for the discretization of $\mathcal{L}$. The implicit scheme is unconditionally stable, while the stability condition for the explicit method is given by $\Delta_t \le \frac{\Delta_x^2}{2\sup a}$ and $\Delta_x < 2$ (cf. [7]).

In the Appendix we formulate the discretization of the PDE (2.2) by means of (2.14), as the block bi-diagonal linear system (A.4). It is remarkable that the solution of such a system only requires the inversion of a tri-diagonal matrix which can be computed very efficiently.

2.2 Calibration and continuous dependence results

In the calibration procedure, we consider a volatility σ (smoothly) depending on a parameter vector $\alpha \in \mathbb{R}^p_+$ for some $p \in \mathbb{N}$: more precisely, we assume that $\sigma = \sigma(d;\alpha) \in C^1(\mathbb{R}\times\mathbb{R}^p_+)$ and that there exist two positive constants C_1, C_2 such that

$$C_1 \le \sigma(d,\alpha) \le C_2, \qquad |\partial_{\alpha_k}\sigma(d,\alpha)| \le C_2 \qquad \forall (d,\alpha) \in \mathbb{R}\times\mathbb{R}^p_+, \quad k = 1,\dots,p.$$

Thus we rewrite the dynamics (1.2) of the price as

$$dS_t = \mu(D_t)S_t dt + \sigma(D_t;\alpha)S_t dW_t, \tag{2.16}$$

and denote by $u(\cdot;\alpha)$ the solution to (2.2)-(2.5) with $a(x,y;\alpha)=\frac{\sigma^2(x-y;\alpha)}{2\lambda}$. For what follows, it will be useful to compute the derivatives of u w.r.t the parameters α. These play the role of the Vega in the standard Black&Scholes approach. A linear system, similar to (A.4), derives from the discretization of the corresponding PDE. Indeed the following result about continuous dependence w.r.t. parameters holds.

Theorem 2.2. *Let $\mathcal{L}^{(\alpha)}$ be the operator in (2.2) with diffusion coefficient $a(\cdot;\alpha)$ and consider the solution u to the Cauchy problem*

$$\begin{cases}\mathcal{L}^{(\alpha)}u(\cdot;\alpha)=0, & \text{in } \mathbb{R}^2\times]0,\lambda T[,\\ u(x,y,0;\alpha)=u_0(x,y), & \text{in } \mathbb{R}^2,\end{cases} \tag{2.17}$$

where the initial datum u_0 is Hölder continuous and such that $|u_0(x,y)|\le C_3e^{C_4(x^2+y^2)}$ with C_4 suitably small. Then, $u(z;\cdot)\in C^1(\mathbb{R}^p_+)$ for every $z=(x,y,t)\in\mathbb{R}^2\times[0,\lambda T]$. Moreover for $k=1,\dots,p$, the derivative $v=\partial_{\alpha_k}u(\cdot;\alpha)$ satisfies the PDE

$$\mathcal{L}^{(\alpha)}v=-(\partial_{\alpha_k}a(\cdot;\alpha))(\partial_{xx}u(\cdot;\alpha)-\partial_xu(\cdot;\alpha)), \tag{2.18}$$

in $\mathbb{R}^2\times]0,\lambda T[$, with initial condition

$$v(x,y,0)=0,\qquad \text{for } (x,y)\in\mathbb{R}^2. \tag{2.19}$$

The proof of the theorem is based on the following

Lemma 2.3. *Under the above assumptions, $\partial_xu,\partial_{xx}u$ are continuous functions w.r.t. the variables (x,y,t,α) and there exist some positive constants C_5,C_6 and $\delta>0$, only dependent on $C_1,\dots,C_4$ and the Hölder constant of u_0, such that*

$$|\partial_xu(x,y,t;\alpha)|+|\partial_{xx}u(x,y,t;\alpha)|\le C_5\frac{e^{C_6(x^2+y^2)}}{t^{1-\delta}}, \tag{2.20}$$

for every $(x,y,t)\in\mathbb{R}^2\times]0,\lambda T[$ and $\alpha\in\mathbb{R}^p_+$.

The proof of Lemma 2.3 is rather delicate since requires the study of some singular integrals. We only mention that the continuity of ∂_xu and $\partial_{xx}u$ can be proved by using the techniques in [10] (see, in particular, Chap. 5 regarding some potential estimates) and estimate (2.20) can be proved as Theorem 8.2, Chap. V in [11], by using the pointwise estimates for the fundamental solution and its derivatives provided in [10], Theorem 1.4. We refer to the forthcoming paper [9] for a detailed proof.

Proof of Theorem 2.2. Let us only consider the case $p=1$. We set $z=(x,y,t)\in\mathbb{R}^2\times]0,\lambda T[$ and denote by $\Gamma^{(\alpha)}$ the fundamental solution of $\mathcal{L}^{(\alpha)}$. Since $v(z)\equiv u(z;\alpha)-u(z;\alpha_0)$ is solution to the problem

$$\begin{cases}\mathcal{L}^{(\alpha_0)}v=-(a(\cdot;\alpha)-a(\cdot;\alpha_0))(\partial_{xx}u(\cdot;\alpha)-\partial_xu(\cdot;\alpha)), & \text{in } \mathbb{R}^2\times]0,\lambda T[,\\ v(x,y,0)=0, & \text{in } \mathbb{R}^2,\end{cases}$$

we have

$$\frac{u(z;\alpha)-u(z;\alpha_0)}{\alpha-\alpha_0}=\int_0^t\int_{\mathbb{R}^2}\Gamma^{(\alpha_0)}(z;\xi,\eta,s)\frac{a(\xi,\eta;\alpha)-a(\xi,\eta;\alpha_0)}{\alpha-\alpha_0}(\partial_{\xi\xi}-\partial_\xi)u(\xi,\eta,s;\alpha)d\xi d\eta ds.$$

Therefore, as α goes to α_0, by the dominated convergence theorem combined with Lemma 2.3, we infer that u is differentiable w.r.t. α and it holds

$$\partial_\alpha u(z;\alpha_0) = \int_0^t \int_{\mathbb{R}^2} \Gamma^{(\alpha_0)}(z;\xi,\eta,s)\partial_\alpha a(\xi,\eta;\alpha_0)(\partial_{\xi\xi} - \partial_\xi)u(\xi,\eta,s;\alpha_0)d\xi d\eta ds.$$

This concludes the proof. □

2.3 Boundary conditions

The numerical solution of (2.2) by finite-difference methods requires the discretization of the equation in a bounded region and the specification of some initial-boundary conditions. More precisely, we approximate the Cauchy problem (2.2)-(2.5) in the cylinder

$$Q = \{(x,y,t) \ | \ |x| < \mu, \ |y| < \nu \ \text{ and } \ 0 < \tau < \lambda T\}, \tag{2.21}$$

for some suitably large μ, ν. By transformation (2.3), this corresponds to the initial-boundary value problem for (1.4) in the domain

$$\{(S,M,t) \ | \ Ke^{-\mu-rt} < S < Ke^{\mu-rt}, \ |M| < \nu \ \text{ and } \ 0 < t < T\}.$$

The conditions on the parabolic boundary of Q, defined by

$$\partial_P Q = \partial Q \cap \{(x,y,t) \ | \ \tau < \lambda T\},$$

are set as follows:

$$u(x,y,0) = (e^x - 1)^+, \qquad \text{for } \ x \in [-\mu,\mu], \ y \in [-\nu,\nu]; \tag{2.22}$$

moreover, we set

$$(\partial_{xx}u - \partial_x u)(\pm\mu,y,t) = 0, \qquad \text{for } \ y \in]-\nu,\nu[, \ t \in]0,\lambda T[. \tag{2.23}$$

We note explicitly that (2.23) corresponds to condition $\partial_{SS} f = 0$ in the original variables, which is somehow standard in the Black&Scholes framework.

It is remarkable that the approximation of $\mathcal{L}$ by its main derivatives allows to avoid imposing conditions on the lateral boundary $\{y = \pm\nu\}$, provided that ν is suitably large. To be more specific, let us first introduce some notation. Fixed $i_0, j_{0,n} \in \mathbb{N}$ for $n \in \mathbb{N} \cup \{0\}$, we denote

$$u^n_{i,j} = u(i\Delta_x, j\Delta_y, n\Delta_t), \qquad i,j \in \mathbb{Z}, \quad |i| \le i_0, \quad |j| \le j_{0,n}. \tag{2.24}$$

Applying the discrete operator in (2.10) to $u^n_{i,j}$ for $|i| \le i_0 - 1$ gives

$$D_{\Delta_x^2} u^n_{i,j} - D_{\Delta_x} u^n_{i,j} = (d_1 u^n_{i-1,j} + d_2 u^n_{i,j} + d_3 u^n_{i+1,j}). \tag{2.25}$$

Consider now the discretization (2.12) and assume that $(x,y,t) = (i\Delta_x, j\Delta_y, n\Delta_t)$ belongs to the grid. Then we have

$$\widetilde{u}(x, y + (x-y)\Delta_t, t - \Delta_t) = (1-\gamma)\, u^{n-1}_{i,j+k} + \gamma\, u^{n-1}_{i,j+k+1}$$

and

$$Y^-_{\Delta_t} u^n_{i,j} = \frac{1}{\Delta_t}\left(u^n_{i,j} - (1-\gamma)u^{n-1}_{i,j+k} - \gamma u^{n-1}_{i,j+k+1}\right), \tag{2.26}$$

where k and γ are, respectively, the integer and fractional part of $(x-y)\Delta_t/\Delta_y$, that is

$$k = \left[\frac{(x-y)\Delta_t}{\Delta_y}\right] = \left[\left(i\frac{\Delta_x}{\Delta_y} - j\right)\Delta_t\right] \qquad \text{and} \qquad \gamma = \left|\frac{(x-y)\Delta_t}{\Delta_y} - k\right|. \tag{2.27}$$

Applying the discrete operator $\mathcal{L}^-_G$ to $u^n_{i,j}$ reads

$$a_{ij}\left(D_{\Delta_x^2} u^n_{i,j} - D_{\Delta_x} u^n_{i,j}\right) + Y^-_{\Delta_t} u^n_{i,j} = 0, \qquad |i| \le i_0 - 1,\ |j| \le j_{0,n}, \tag{2.28}$$

where $a_{ij} = a(i\Delta_x, j\Delta_y)$. On the other hand, assuming $\mu = i_0\Delta_x$, condition (2.23) is equivalent to

$$Y^-_{\Delta_t} u^n_{i,j} = 0, \qquad i = \pm i_0,\ |j| \le j_{0,n}. \tag{2.29}$$

Next we fix $j_{0,N} \in \mathbb{N}$ and examine the domain of dependence of the set of values

$$U_N = \left\{u^N_{i,j} \mid \quad |i| \le i_0,\ |j| \le j^N_0\right\};$$

more precisely, for $0 \le n \le N-1$, we specify $j_{0,n}$ as the maximum of the set of the indexes j's such that U_N depends on $u^n_{i,j}$ through conditions (2.28)-(2.29). Moreover we set $\nu_n = j_{0,n}\Delta_y$. Since, by (2.26) and (2.27), it holds

$$j_{0,n-1} = j_{0,n} + \left[j_{0,n}\Delta_t + i_0\frac{\Delta_x\Delta_t}{\Delta_y}\right] + 1 \le j_{0,n}(1+\Delta_t) + i_0\frac{\Delta_x\Delta_t}{\Delta_y} + 1,$$

it follows that

$$\nu_{n-1} \le \nu_n(1+\Delta_t) + \mu\Delta_t + \Delta_y$$

and thus $\nu_{N-n} \le z_n$, where z_n is defined by the difference equation

$$z_{n+1} = (1+\Delta_t)z_n + \mu\Delta_t + \Delta_y, \qquad\qquad z_0 = \nu_N,$$

which has solution $z_n = (1+\Delta_t)^n(y_0 + \mu + \Delta_y/\Delta_t) - \mu - \Delta_y/\Delta_t$: indeed, recall that the solution of the difference equation $z_{n+1} = \alpha z_n + \beta$, with initial value z_0 and $\alpha \neq 1$, is given by $z_n = \alpha^n(z_0 - z_*) + z_*$, where $z_* = \beta/(1-\alpha)$ the equilibrium value. Finally, we deduce

$$\nu_n = (1+\Delta_t)^{(N-n)}\left(\nu_N + \mu + \Delta_y/\Delta_t\right) - \mu - \Delta_y/\Delta_t$$

and

$$\begin{aligned}\nu_0 &= (1+\Delta_t)^{\lambda T/\Delta_t}\left(\nu_N + \mu + \Delta_y/\Delta_t\right) - \mu - \Delta_y/\Delta_t \\ &\le e^{\lambda T}\nu_N + (e^{\lambda T} - 1)(\mu + \Delta_y/\Delta_t).\end{aligned}$$

Thus we have proved the following result.

Theorem 2.4. *Assume that*

$$\frac{\Delta_y}{\Delta_t} = C_0, \tag{2.30}$$

for some constant C_0. Then, in order to approximate the solution $u(x, y, \lambda T)$ for $|x| \le \mu$ and $|y| \le \nu_N$, conditions on the lateral boundary $\{y = \pm\widetilde{\nu}\}$, where $\widetilde{\nu} = e^{\lambda T}\nu_N + (e^{\lambda T} - 1)(\mu + C_0)$, are superfluous.

Remark 2.5. *Notice that, under condition* (2.30)*, the approximation error of $\mathcal{L}_G^{\pm}$ in* (2.15) *reduces to an order of $\Delta_x^2 + \Delta_t$.*

Moreover, condition (2.30) *ensures that the width of the initial region can be chosen independently of the refinement of the grid. Alternatively, one can solve* (2.2) *on the prism*

$$\{(x, y, t) \mid \quad |x| < \mu,\ |y| < e^{\lambda T - t}\nu_N + (e^{\lambda T - t} - 1)(\mu + C_0),\ 0 < t < \lambda T\},$$

rather than on the whole cylinder Q.

3 Calibration

The calibration of the HR model consists in determining the volatility function σ from observed market prices of European options. Actually, we only look for the function σ in (2.4) for which the PDE (2.2) best approximates the observations. Indeed the presence of pricing errors, inconsistencies and/or inefficiency in the market may not allow to fit exactly the data. Moreover u is observed only at a finite number of points, thus specific restrictions should be imposed on σ in order to obtain a well posed problem.

In general, we assume that $\sigma = \sigma(\cdot; \alpha)$ depends on a vector $\alpha = (\alpha_1, \ldots, \alpha_p)$ of real positive parameters and denote by $u(x, y, t; \alpha)$ the solution to the Cauchy problem for (2.2)-(2.5) corresponding to $\sigma(\cdot\,; \alpha)$. This defines a mapping from $\mathbb{R}_+^p$ to $C^\infty(\mathbb{R}^2 \times]0, \lambda T[)$. The scope of this section is to develop and test a numerical procedure to "invert" that function.

Let $\hat{f}_i$ be the observed option value at the point $z_i \equiv (x_i, y_i, t_i)$, for $i = 1, 2, \ldots, M$, and let $f_i(\alpha)$ be the price given by (2.3) in terms of the solution $u(x_i, y_i, t_i; \alpha)$ of the PDE (2.2) for a given α at the observation point z_i. Since the point z_i may not belong to the grid G, the value of $f_i(\alpha)$ is approximated by using a linear interpolation of the nearest points of the grid. The error made in fitting the i-th observed value for a given α is denoted by

$$\varepsilon_i(\alpha) = f_i(\alpha) - \hat{f}_i.$$

We aim to find α that best fits the data by solving the nonlinear least squares (NLLS) problem

$$\min_{\alpha \in \mathbb{R}_+^p} \sum_{i=1}^{M} \varepsilon_i^2(\alpha)/w_i \tag{3.1}$$

where w_i is some weight given to the i-th observation. The NLLS problem (3.1) is solved using the Matlab routine `lsqnonlin` which is a trust-region method based on the interior-point method described in [6]. The algorithm needs the first order derivatives $\partial_{\alpha_k} u$ at the points z_i, $(i = 1, \ldots, M)$ which are computed by solving a set of $p + 1$ PDEs (2.2) and (2.18): thus the computational cost linearly increases with the number p of parameters involved.

3.1 The dataset

The calibration procedure here described is applied to a set of European options quotations on the S&P 500 index from the Chicago Board Options Exchange (CBOE). Only calls with time-to-maturity from two weeks to six months are considered, moreover the average of bid and ask prices is used as reference. Observations have been taken each 15 minutes from 11:00 to 14:00 of each trading day in the period from Nov-15-2002 to May-23-2003. The distribution of this dataset, which contains 190397 observations, w.r.t. absolute time, deviation from the trend, time-to-maturity and moneyness is shown in Figure 1.

Following Ait-Sahalia and Lo [1] we do not use quotations on the underlying S_t and realized dividends δ_t, because the first ones are affected by synchronization errors and the second ones are not necessarily equal to the expected rates at the time the option is priced. In order to avoid pricing anomalies that can arise from these problems the following procedure is used: at each time t and for each maturity T and strike K, in order to avoid arbitrage opportunities, the following parity relations hold:

$$F_{T-t} = S_t e^{(r_{t,T}-\delta_{t,T})(T-t)},$$

and

$$U^{call}_{T-t}(S_t, K, r_{t,T}, \delta_{t,T}) + Ke^{-r_{t,T}(T-t)} = U^{put}_{T-t}(S_t, K, r_{t,T}, \delta_{t,T}) + F_{T-t}e^{-r_{t,T}(T-t)},$$

where $F_{T-t}, U^{call}_{T-t}, U^{put}_{T-t}$ denote the future, call and put prices with expiration at T, $r_{t,T}$ and $\delta_{t,T}$ the corresponding interest and dividend rates. Thus, future prices can be inferred from synchronous quotations of put and call options with the same strike and maturity. In order to obtain reliable values, F_{T-t} is computed as the weighted average of the implied futures over all the available strikes. Log of volumes plus one are used as weights, even if a simple average produce similar results. Next, in order to reduce the number of input parameters of the calibration procedure, we use the homogeneity relation

$$e^{r_{t,T}(T-t)}U_{T-t}(S_t, K, r_{t,T}, \delta_{t,T}) = U_{T-t}(F_{T-t}, K, 0, 0) = f(F_{T-t}, M_t, T-t),$$

to replace the option prices $U(S_t, K, r_{t,T}, \delta_{t,T})$ with the ex-rates prices $U(F_{T-t}, K, 0, 0)$: this corresponds to the change of variables in (1.3).

Notice that many authors modify each cross section before the calibration. For example in [4] implied volatilities curves are computed by smoothing splines from market observations and in [2] constrained cubic splines are used to smooth market prices and to enforce non-arbitrage conditions. In both the cases the reported results refer to the modified values. Here, we only infer the underlying future price and *use raw data for the fitting.* Furthermore, differently from other investigations, where transactions or daily closing prices are used, we use a dataset built from intra-day observation of bid-ask prices which are not necessarily near to some transaction.

To compute the exponential trend M_t and the corresponding deviation D_t we have used closing day prices from October 1982 to September 2002 and then intra-day prices until May 2003. Index and trend computed with $\lambda = 1$ are shown in Figure 2. We have chosen $\lambda = 1$ as it gives the best reproduction of the term structure of implied volatilities. The period considered in the dataset has an initial decreasing phase followed by sharp rise of the index level.

The dependency of the option prices on D_t is evident from Figure 3. The four panels plot the implied volatilities against the adjusted log-moneyness $\log(F/K)/\sqrt{T-t}$: as it was noted by Foque et al. [15] the implied volatility smile of a cross section of index options is a function of $\log(F/K)/\sqrt{T-t}$ only. This relation captures the term structure of option implied volatilities. Each panel refer to a different range of D_t. The minimum of the smile curve moves down from an implied volatility of 0.22 to one of 0.15 and move left from a log-moneyness of -0.5 to one of -0.25. Notice that, the observations of D_t, like S_t, are affected by errors, due to synchronization or to market inefficiencies.

3.2 Calibration results

Since the observations are not homogeneously distributed w.r.t. time-to-maturity, moneyness and deviation from the trend, we adopt the following strategy to choose the weights w_i in the (3.1). We divide option transactions in 18 groups based on maturity ($[0,3]$ or $]3,6]$ months), log-moneyness ($]-\infty,-.1]$, $]-.1,.1]$ and $].1,\infty[$) and deviation from trend ($]-\infty,-.2]$, $]-.2,-.15]$, $]-.15,-.1]$, $]-.1,\infty]$). The weight w_i of the ith observation has been chosen equal to the number of elements in the corresponding group.

The HR model have been calibrated to the data for two different choices of the volatility function $\sigma^2(D)$. Following [16], the first choice consists in a piecewise cubic Hermite polynomial $\sigma^2_{Spline}(D)$ interpolating the abscissae $\sigma^2_{Spline}(D_i) = \alpha_i$, for $1 \le i \le 7$ at the knots $D_i \in \{-1, -2/3, -1/3, 0, 1/3, 2/3, 1\}$. See Figure 4, where the interpolating polynomial and the knots are represented by a dashed line and by circles, respectively. The function $\sigma^2_{Spline}(D)$ is chosen linear outside the interval $[-1,1]$ continuous up to the first derivative in $D = 1$ and $D = -1$. Further, its positiveness is ensured by the constrains $\alpha_i \ge 0$, $1 \le i \le 7$, in the NLLS problem (3.1). Hereafter, we refer to this function as the *Spline volatility function* and to the corresponding model as the *Spline model*.

The second choice consists in

$$\sigma^2_{HR}(D) = \min\left\{\alpha_1 + \alpha_2(D-\alpha_3)^2, \sqrt{5}\right\},$$

with the constraints $\alpha_i \ge 0$, for $i = 1, 2$ and α_3 unconstrained. We refer to this function as the *HR volatility function* and to the corresponding model the *HR model*. The calibrated parameters of the two functions and their standard deviations are reported in Table 1. Figure 4 shows the graphs of the two volatility functions.

In order to overcome possible observation or model errors in D_t, we have re-calibrated the offset parameter α_3 of the HR model for each day of the dataset. More precisely, the parameters α_1 and α_2 have been kept fixed to the previously estimated values, that is to the values reported in Table 1 and the parameter α_3 is calibrated using the observations of each given day: this, results in a series of estimates $\alpha_t^{(3)}$ which allows to recover the option implied deviations defined by $\widetilde{D}_t = D_t + \alpha_3 - \alpha_t^{(3)}$. The two time-series D_t and $\widetilde{D}_t$ are shown in Figure 5, where it can be noticed that the difference is often substantial. We refer to this calibration as the *HR re-calibrated model*.

To analyze the quality of the fit, four kinds of errors are considered:

- absolute or dollar (valuation) error: $\varepsilon_i = f_i - \hat{f}_i$;
- percentage or relative error: $\hat{\varepsilon}_i = \varepsilon_i / \hat{f}_i$;

- error outside the bid-ask spread, or simply outside error:

$$\varepsilon_i^{OE} = \text{sign}(\varepsilon_i)\max(f_i - \hat{f}_i^{ask}, \hat{f}_i^{bid} - f_i, 0);$$

- percentage or relative outside error: $\hat{\varepsilon}_i^{OE} = \varepsilon_i^{OE}/\hat{f}_i$;

where $\hat{f}_i^{ask}$ and $\hat{f}_i^{bid}$ are the bid and ask prices of the ith observation (cf. [12]). In order to partially eliminate the bias in percentage errors, only calls with price larger than 10\$ are considered when computing statistics for relative errors (note that the value of the underlying is 887\$ in mean).

Table 2 contains the following resuming statistics for the three models and the four types of errors: mean error, standard deviation, extreme values, Root Mean Square Error (RMSE)

$$\text{RMSE}(\varepsilon_i) = \left(M^{-1} \sum_{i=1}^{M} \varepsilon_i^2 \right)^{1/2}$$

and the Mean Absolute Error (MAE),

$$\text{MAE}(\varepsilon_i) = M^{-1} \sum_{i=1}^{M} |\varepsilon_i|.$$

The four panels in Figures 6 and 7, respectively, plot the RMSEs of absolute and relative outside errors for different ranges of absolute time, deviation from the trend, time-to-expiration and moneyness.

Let first compare the fits of the HR and Spline specifications. The overall performances of both models are good, also considering the length of the period and that the volatility function, and thus the pricing kernel, is kept constant. The good results are confirmed by the histograms of absolute and percentage errors for the HR and Spline calibrations shown in Figure 8. From the third panel of Figures 6 and 7 it should be noticed that both the models well explain the term-to-maturity structure of option prices. This has been pointed as a deficit of stochastic volatility models in [15, 17, 21].

The Spline model obtains slightly better results than those of the HR model, but the difference is so small that the HR model is preferred for its parsimony. It can be seen from Figure 4 that the two volatility functions differ only on their tails and especially on the right ones. However, as indicated by the standard deviations reported in Table 1, σ^2_{Spline} is completely imprecise in that region. In fact, the last two parameters of σ^2_{Spline} are not identifiable because they do not significantly affect the solution $u(x, y, t)$ of (2.2) on the observation points.

Now, let discuss the performance of the HR re-calibrated model. This approach allows for a further improvement in the fit: both the absolute and relative outside errors are reduced of one third (see Table 2). Furthermore, implying D_t from option prices allows to better capture the term structure of option prices (see third panel in Figures 6 and 7). While the distribution of the HR and Spline models, shown in Figure 8 is clearly not normal, that of the HR re-calibrated model follows a normal one. This should point out a misspecification of D_t in the HR and Spline models that almost disappears in the HR re-calibrated model. This also suggests that further investigation in the model w.r.t. to the specification of the state variables D_t is needed. Here

we mention the model suggested by Hubalek et al. [19] or the possible adding of an additional deviation $D_{\lambda_2,t}$ with a faster decay (a shorter memory) or a second order offset function

$$D_t^{(2)} \equiv \int_0^\infty \lambda e^{-\lambda\tau}(Z_t - Z_{t-\tau})^2 d\tau,$$

as already considered in [18], to better explain the market behavior.

Figure 9 shows implied volatilities for the HR model using the daily calibrated deviations $\widetilde{D}_t$. As can be seen by comparing Figures 3 and 9, the model is not able to fully reproduce the smiles for deep in- or out-of-the money options. Furthermore, smiles implied by the market are more significant especially for shorter maturities, as it was indicated by Hubalek et al. [19].

3.3 Out-of-sample tests

In order to test out-of-sample performances, the HR model have been calibrated on the observations ranging from Nov-15-2002 to Jan-14-2003 and tested on the successive week, month and three months periods. The calibration produces the volatility function

$$\sigma_{HR}(D)^2 = 0.0297 + 0.9360(D - 0.0352)^2$$

and examples of the in- and out-of-sample fits are shown in Figure 10, where the calibrated payoffs for different maturities are represented by the curves and market prices $\hat{f}_i$ by the crosses.

Statistics for in-sample and out-of-sample tests are given in Table 3 and RMSEs are plotted against time, deviation, maturity and log-moneyness in Figure 11. As expected, out-of-sample performances get worse as the horizon considered increases. Moreover, since the calibration is performed mainly on short maturity options it does not give a very good prediction for longer maturities. Nevertheless the RMSEs in the first panel follow the same pattern of the RMSEs in Figure 6, with an exception at week 17. Table 3 also confirms the validity of the model which, contrary to local volatility models, seems to have a good performance even if it is not continuously re-calibrated. In particular, the quality of the fit seems to be quite acceptable even one month after the calibration period, confirming the theoretical arguments.

A Appendix: discretization and linear systems

Throughout this Appendix we use the notations of Subsection 2.3. The aim is to formulate the discretization of the partial differential equation (2.2) as a block bidiagonal linear system. We define $I = 2i_0 + 1$, $J_n = 2j_{0,n} + 1$ and denote by $u^n \in \mathbb{R}^{IJ_n}$ the vector containing the values $u^n_{i,j}$ for $|i| \leq i_0$ and $|j| \leq j_{0,n}$: those values are sorted by the couple of indices (j, i) in lexicografic order.

Let consider now, the application of the discrete operator $Y^-_{\Delta_t}$ in (2.26) to the vector u^n. The generic element $Y^-_{\Delta_t} u^n_{i,j}$ is the linear combination of the corresponding element in u^n and two elements, $u^{n-1}_{i,j+k}$ and $u^{n-1}_{i,j+k+1}$ of u^{n-1}. Thus, applying $Y^-_{\Delta_t}$ to u_n is equivalent to the difference of two linear operators, $\Delta_t^{-1}\mathcal{I}_\backslash$ and $\Delta_t^{-1} Z_n$, applied respectively to u^n and u^{n-1}, where $\mathcal{I}_\backslash$ denotes the identity operator in $\mathbb{R}^{IJ_n}$. Specifically, the vector with elements $Y^-_{\Delta_t} u^n_{i,j}$ is given by

$$\frac{1}{\Delta_t}(u^n - Z_n u^{n-1}),$$

where $Z_n \in \mathbb{R}^{IJ_n \times IJ_{n-1}}$ is the matrix such that the entry corresponding to the index i, j of Zu^{n-1} is given by

$$(1-\gamma)u_{i,j+k}^{n-1} + \gamma u_{i,j+k+1}^{n-1}.$$

Then it turns out that the linear system (2.28) can be rewritten in matrix form

$$(\mathcal{I}_n + \Delta_t A_n D_n)u^n - Z_n u^{n-1} = 0, \tag{A.1}$$

for $1 \le n \le N$, where $A \in \mathbb{R}^{IJ_n \times IJ_n}$ is the diagonal matrix with elements a_{ij} and

$$D_n = \begin{pmatrix} \check{D} & 0 & \cdots & 0 \\ 0 & \check{D} & \cdots & 0 \\ \vdots & \vdots & \ddots & \vdots \\ 0 & 0 & \cdots & \check{D} \end{pmatrix} \qquad \text{and} \qquad \check{D} = \begin{pmatrix} 0 & 0 & 0 & \cdots & 0 \\ d_1 & d_2 & d_3 & \cdots & 0 \\ 0 & \ddots & \ddots & \ddots & \vdots \\ 0 & \cdots & d_1 & d_2 & d_3 \\ 0 & \cdots & 0 & 0 & 0 \end{pmatrix}, \tag{A.2}$$

are tridiagonal matrices of order IJ_n and I, respectively.

Similarly, combining the forward and backward schemes allows to derive the θ-method:

$$\theta\Delta_t A_n D_n u^n + (1-\theta)\Delta_t Z_n A_{n-1} D_{n-1} u^{n-1} - Z_n u^{n-1} + u^n = 0,$$

or

$$\bar{A}_1^n u^n = \bar{A}_2^n u^{n-1}, \qquad 1 \le n \le N, \tag{A.3}$$

with $\bar{A}_1^n = (\mathcal{I}_n + \theta\Delta_t A_n D_n)$ and $\bar{A}_2^n = Z_n(\mathcal{I}_n - (1-\theta)\Delta_t A_{n-1} D_{n-1})$. As usual, the θ-method reduces to the explicit, implicit or Crank-Nicholson schemes when $\theta = 0, 1$ or 0.5, respectively. Notice that the θ-method is unconditionally stable for $0.5 \le \theta \le 1$. The matrices $\bar{A}_1^n$ and D_n have an identical structure, specifically they are block diagonal with tridiagonal blocks. Thus, the computational cost required to solve (A.3) is of the order of IJ_n. Furthermore, the structure of the matrices can be exploited to design computationally efficient and/or parallel algorithms for the solution of the PDE (2.2).

Finally, by setting $N = \lambda T/\Delta_t$ it turns out that considering (A.3) for $n = 1, \ldots, N$ and imposing the initial conditions $u_0 = v_0$ is equivalent to the linear system

$$\begin{pmatrix} I & 0 & 0 & \cdots & 0 \\ -\bar{A}_2^1 & \bar{A}_1^1 & 0 & \cdots & 0 \\ \vdots & \ddots & \ddots & & \vdots \\ 0 & \cdots & -\bar{A}_2^{N-1} & \bar{A}_1^{N-1} & 0 \\ 0 & \cdots & 0 & -\bar{A}_2^N & \bar{A}_1^N \end{pmatrix} \begin{pmatrix} u^0 \\ u^1 \\ \vdots \\ u^{N-1} \\ u^N \end{pmatrix} = \begin{pmatrix} v^0 \\ 0 \\ \vdots \\ 0 \\ 0 \end{pmatrix}$$

or, with the appropriate substitution,

$$\bar{A}\bar{u} = \bar{v}, \tag{A.4}$$

where $\bar{A}$ is block bidiagonal and $\bar{u} \in \mathbb{R}^q$ where

$$q = \sum_{n=0}^{N} IJ_n. \tag{A.5}$$

Existence and uniqueness of the solution are related to the non-singularity of $\bar{A}_1^n$ and, in view of the expressions of d_1, d_2, d_3, are clearly guaranteed if $\frac{\Delta_t}{\Delta_{x^2}}$ is suitably small. Stability and numerical stability are driven by the properties of the matrices $\bar{A}_1^n$ and $\bar{A}_2^n$.

References

[1] Y. Aït-Sahalia and A. W. Lo, *Nonparametric estimation of state-price densities implicit in financial asset prices*, The Journal of Finance, LIII (1998), pp. 499–547.

[2] D. S. Bates, *Post-'87 crash fears in the S&P 500 futures option market*, J. Econometrics, 94 (2000), pp. 181–238.

[3] V. Blaka Hallulli and T. Vargiolu, *Financial models with dependence on the past: a survey*, Applied and Industrial Mathematics in Italy, M. Primicerio, R. Spigler, V. Valente, editors, Series on Advances in Mathematics for Applied Sciences, World Scientific 2005, 69 (2005).

[4] M. Broadie, M. Chernov, and M. Johannes, *Model specification and risk premiums: The evidence fromthe futures options*, tech. report, Columbia University, 2005.

[5] C. Chiarella and K. Kwon, *A complete Markovian stochastic volatility model in the HJM framework*, Asia-Pacific Financial Markets, 7 (2000), pp. 293–304.

[6] T. Coleman and Y. Li, *An interior, trust region approach for nonlinear minimization subject to bounds*, SIAM Journal on Optimization, 6 (1996), pp. 418–445.

[7] M. Di Francesco, P. Foschi, and A. Pascucci, *Analysis of an uncertan volatility model*, Preprint AMS Acta, (2005).

[8] M. Di Francesco and A. Pascucci, *On the complete model with stochastic volatility by Hobson and Rogers*, Proc. R. Soc. Lond. Ser. A Math. Phys. Eng. Sci., 460 (2004), pp. 3327–3338.

[9] M. Di Francesco and A. Pascucci, *A continuous dependence result for ultra-parabolic equations*, Preprint AMS Acta, (2005).

[10] ——, *On a class of degenerate parabolic equations of Kolmogorov type*, AMRX Appl. Math. Res. Express, 3 (2005), pp. 77–116.

[11] E. DiBenedetto, *Partial differential equations*, Birkhäuser Boston Inc., Boston, MA, 1995.

[12] B. Dumas, J. Fleming, and R. E. Whaley, *Implied volatility functions: empirical tests*, J. Finance, 53 (1998), pp. 2059–2106.

[13] B. Dupire, *Pricing and hedging with smiles*, in Mathematics of derivative securities (Cambridge, 1995), vol. 15 of Publ. Newton Inst., Cambridge Univ. Press, Cambridge, 1997, pp. 103–111.

[14] G. Figà-Talamanca and M. L. Guerra, *Complete models with stochastic volatility: further implications*, Working Paper, Università della Tuscia, Facoltà di Economia, 5 (2000).

[15] J.-P. Foque, G. Papanicolau, K. Sircar, and K. Solna, *Maturity cycles in S&P 500 volatility*, Journal of Computational Finance, 6 (2003), pp. 1648–1665.

[16] F. Fritsch and R. Carlson, *Monotone piecewise cubic interpolation*, SIAM Journal on Numerical Analysis, 17 (1980), pp. 238–246.

[17] R. Garcia, E. Ghysels, and E. Renault, *The econometrics of option pricing*, in Handbook of Financial Econometrics, Y. Ait-Sahalia and L. Hansen, eds., 2002. (preliminary version).

[18] D. G. Hobson and L. C. G. Rogers, *Complete models with stochastic volatility*, Math. Finance, 8 (1998), pp. 27–48.

[19] F. Hubalek, J. Teichmann, and R. Tompkins, *Flexible complete models with stochastic volatility generalising Hobson-Rogers*, working paper, (2005).

[20] E. Lanconelli, A. Pascucci, and S. Polidoro, *Linear and nonlinear ultraparabolic equations of Kolmogorov type arising in diffusion theory and in finance*, in Nonlinear problems in mathematical physics and related topics, II, vol. 2 of Int. Math. Ser. (N. Y.), Kluwer/Plenum, New York, 2002, pp. 243–265.

[21] S. Sundaresan, *Continuous-time methods in finance: A review and an assessment*, Journal of Finance, 55 (2000), pp. 1569–1622.

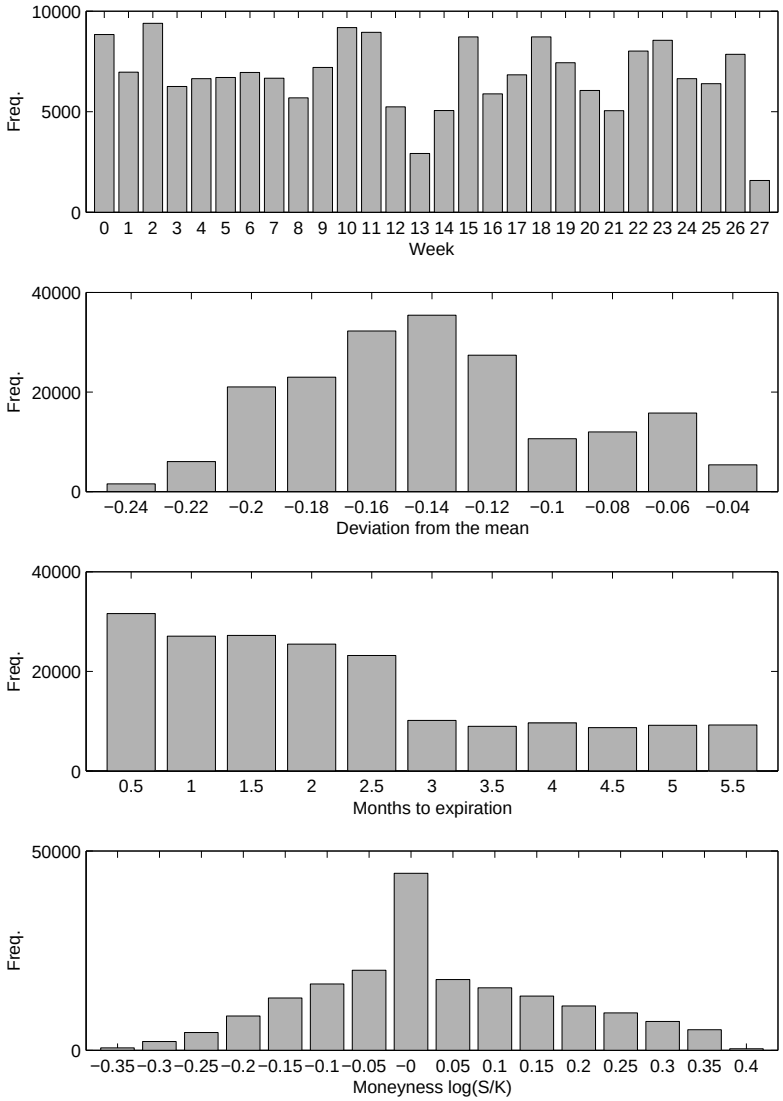

Figure 1: Distribution of observations. The four panels show the number of observations plotted against time (measured in weeks), deviation from the mean, time to maturity (measured in months) and moneyness.

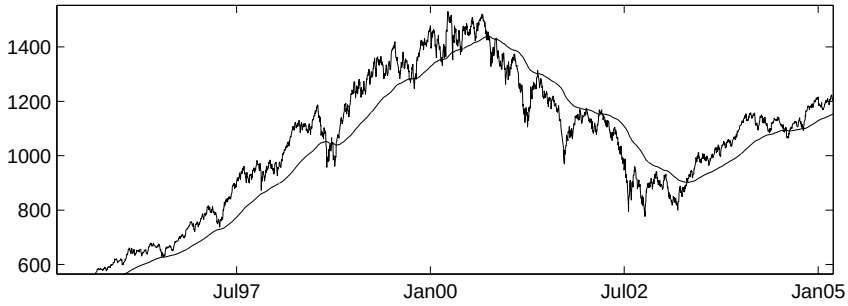

Figure 2: Price of the S&P 500 index S_t and the corresponding exponential trend computed with $\lambda = 1$ for the years 1997-2004.

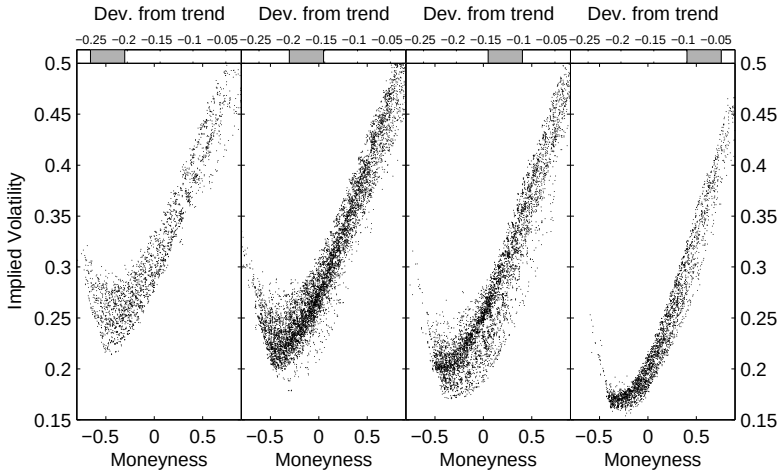

Figure 3: Effects of the deviation from the trend on marked implied volatilities. The implied volatilities are plotted against adjusted log-moneyness $\log(F/K)/\sqrt{T-t}$ and grouped by different ranges of D as shown by the bar in the top of each panel.

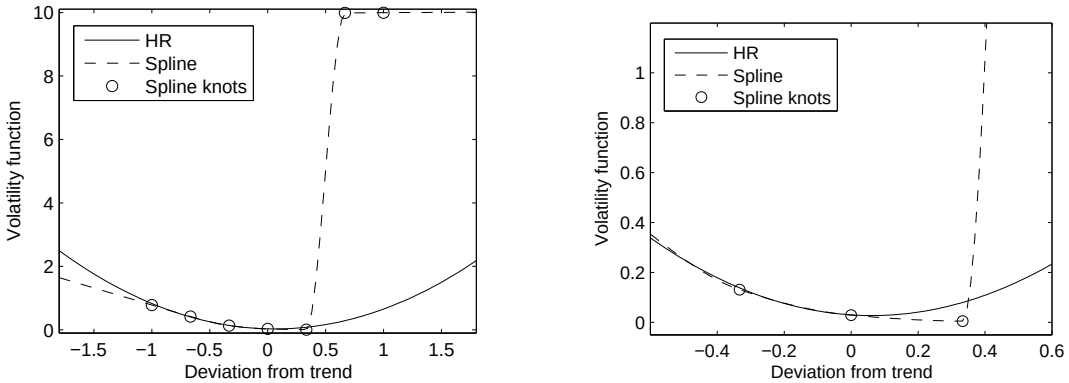

Figure 4: Calibrated Volatility functions σ^2_{HR} and σ^2_{Spline}.

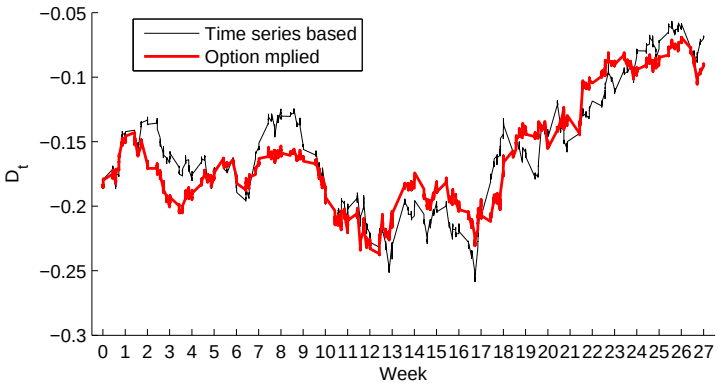

Figure 5: .

	Spline		HR	
	α_i	Std. dev.	α_i	Std. dev.
α_1	0.7791	(3.59e-2)	0.0272	(8.51e-5)
α_2	0.4195	(2.01e-3)	0.7114	(2.11e-3)
α_3	0.1308	(1.24e-4)	0.0616	(6.51e-4)
α_4	0.0289	(4.17e-5)		
α_5	0.0050	(3.54e-4)		
α_6	9.9862	(2.46e+5)		
α_7	9.9927	(6.58e+5)		

Table 1: .

Absolute Errors

Model	RMSE	MAE	Mean	Std. Dev.	Minimum	Maximum
Spline	1.853	1.458	-0.757	1.692	-5.944	7.049
HR	1.857	1.463	-0.789	1.681	-6.113	7.131
HR Recal.	1.532	1.229	-0.613	1.403	-4.948	4.81

Absolute Outside errors

Model	RMSE	MAE	Mean	Std. Dev.	Minimum	Maximum
Spline	1.153	0.740	-0.366	1.094	-5.532	6.043
HR	1.154	0.741	-0.387	1.087	-5.846	6.125
HR Recal	0.852	0.533	-0.271	0.808	-4.131	3.976

Percentage Errors

Model	RMSE	MAE	Mean	Std. Dev.	Minimum	Maximum
Spline	5.16%	3.29%	-0.71%	5.11%	-34.40%	33.08%
HR	5.19%	3.34%	-1.05%	5.09%	-36.56%	32.05%
HR Recal.	4.33%	2.73%	-0.47%	4.30%	-26.00%	34.06%

Percentage Outside Errors

Model	RMSE	MAE	Mean	Std. Dev.	Minimum	Maximum
Spline	3.37%	1.70%	-0.34%	3.35%	-29.57%	29.69%
HR	3.37%	1.73%	-0.56%	3.33%	-31.72%	28.66%
HR Recal.	2.62%	1.19%	-0.26%	2.60%	-23.01%	31.62%

Table 2: Statistics for absolute (relative) errors and outside errors for the calibrations with the Spline, HR and HR re-calibrated models.

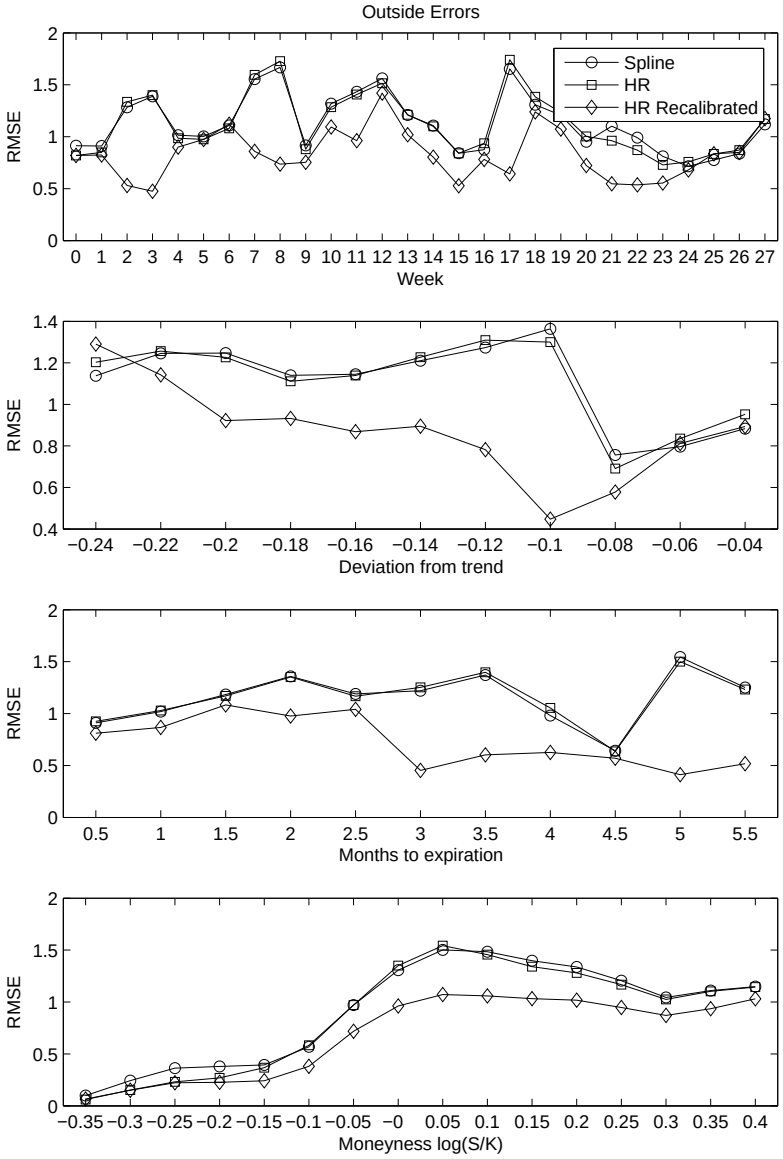

Figure 6: Plot of RMSEs of absolute outside errors against observation time (measured in weeks), deviation from the mean, time to maturity (measured in months) and moneyness. Results for the Spline, HR and HR re-calibrated models are represented by circles, squares and diamond, respectively.

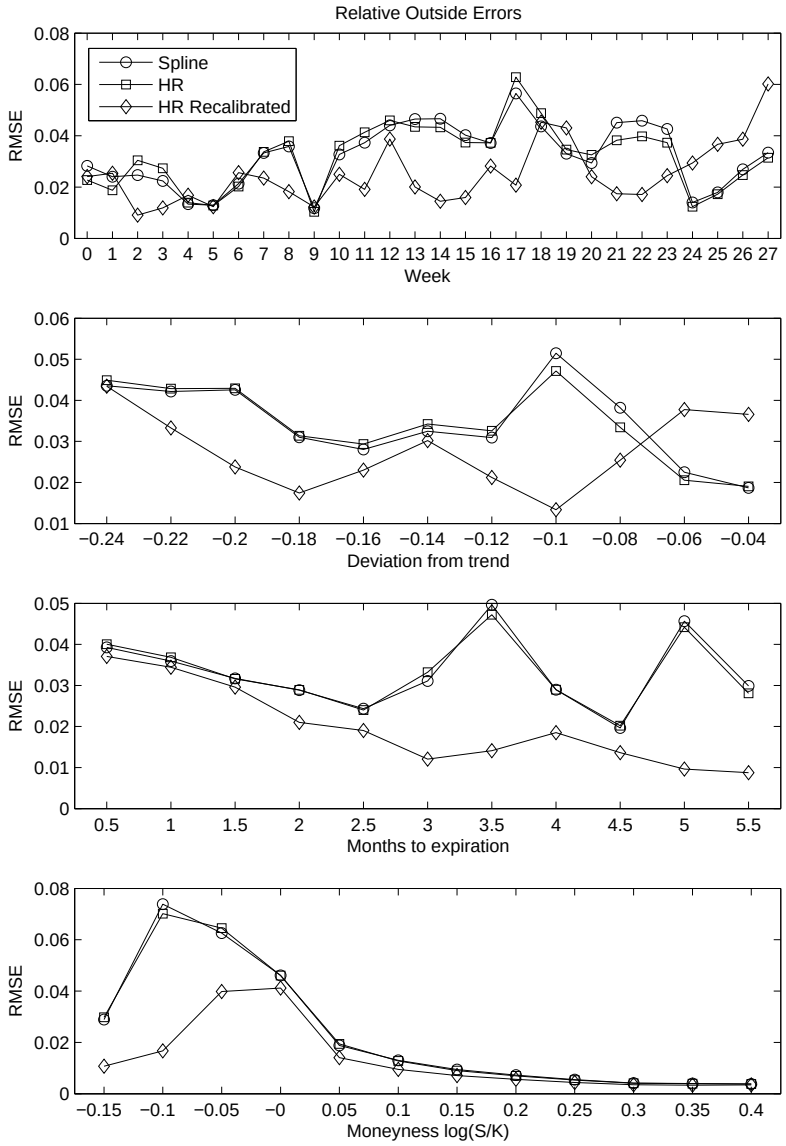

Figure 7: Plot of RMSEs of relative outside errors against observation time (measured in weeks), deviation from the mean, time to maturity (measured in months) and moneyness. Results for the Spline, HR and HR re-calibrated models are represented by circles, squares and diamond, respectively.

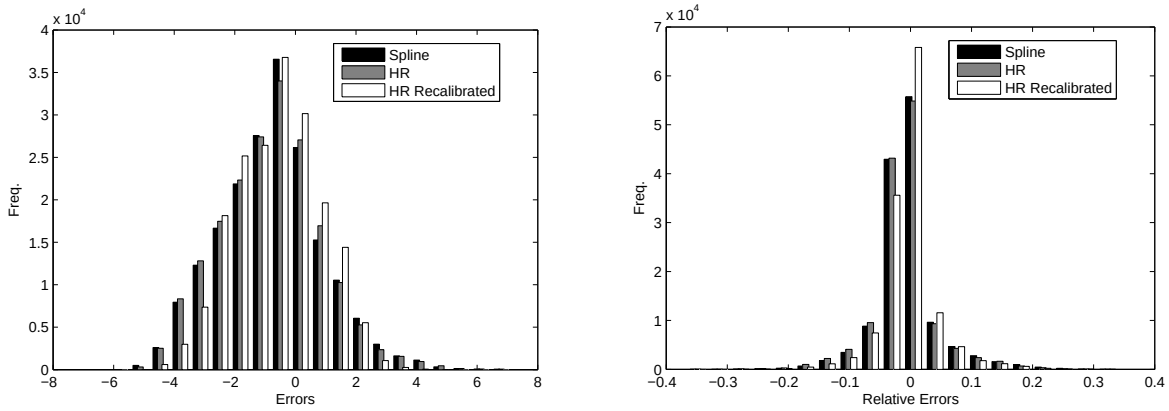

Figure 8: Histograms of the errors in the calibration with the HR and Spline volatility models.

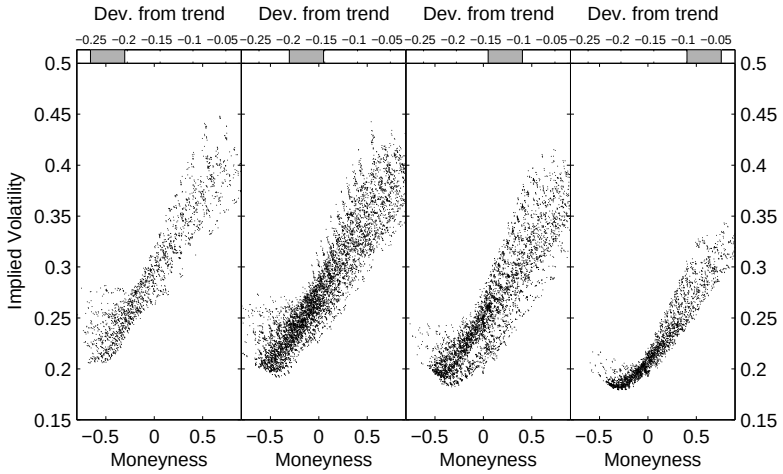

Figure 9: Effects of the deviation from the trend on marked implied volatilities. The implied volatilities are plotted against adjusted log-moneyness $\log(F/K)/\sqrt{T-t}$ and grouped by different ranges of the deviation as shown by the bar at the top of each panel.

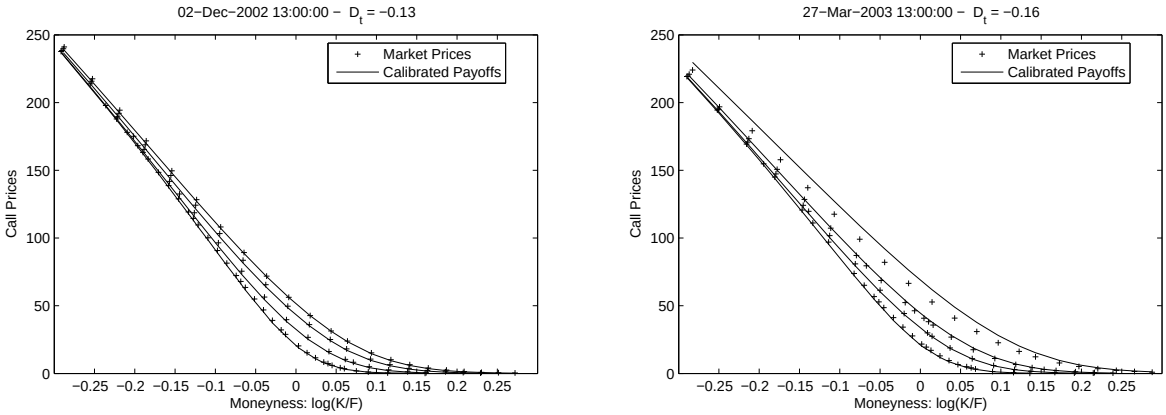

Figure 10: Market prices and call price curves on December 2nd (in sample) and March 27th (out of sample). The calibration has been performed over the period November 15th 2002 - January 14th 2003.

Absolute errors

	RMSE	MAE	Mean	Std. Dev.	Min	Max
in-sample	1.71	1.34	-0.46	1.65	-4.28	7.58
out-of-sample						
1 week	1.58	1.18	-0.02	1.58	-3.17	5.46
1 month	2.23	1.49	0.18	2.22	-3.97	10.51
3 months	2.69	1.75	0.60	2.63	-5.16	13.29

Absolute outside errors

	RMSE	MAE	Mean	Std. Dev.	Min	Max
in-sample	0.99	0.58	-0.07	0.99	-3.29	6.52
out-of-sample						
1 week	0.97	0.54	0.08	0.97	-2.18	4.45
1 month	1.67	0.84	0.35	1.63	-3.03	10.01
3 months	2.13	1.07	0.65	2.02	-5.06	12.28

Percentage errors

	RMSE	MAE	Mean	Std. Dev.	Min	Max
in-sample	4.06%	2.56%	-0.17%	4.06%	-20.17%	33.14%
out-of-sample						
1 week	4.04%	2.64%	1.23%	3.85%	- 5.33%	19.20%
1 month	5.84%	3.78%	1.15%	5.72%	-17.36%	39.71%
3 months	8.19%	4.86%	2.23%	7.88%	-33.17%	48.38%

Percentage outside errors

	RMSE	MAE	Mean	Std. Dev.	Min	Max
in-sample	2.50%	1.14%	0.13%	2.50%	-15.27%	30.35%
out-of-sample						
1 week	2.31%	1.16%	0.71%	2.20%	- 2.16%	14.44%
1 month	4.12%	2.08%	1.16%	3.95%	-14.75%	36.77%
3 months	6.45%	3.16%	2.01%	6.13%	-28.16%	45.26%

Table 3: In-sample and out-of-sample statistics for percentage errors ε_i and absolute errors $\hat{\varepsilon}_i$ of the calibration over the period from Jan-17 to Feb-17-2003. Out-of-sample statistics refers to the one week, one month and three months periods starting the 18-Feb-2003.

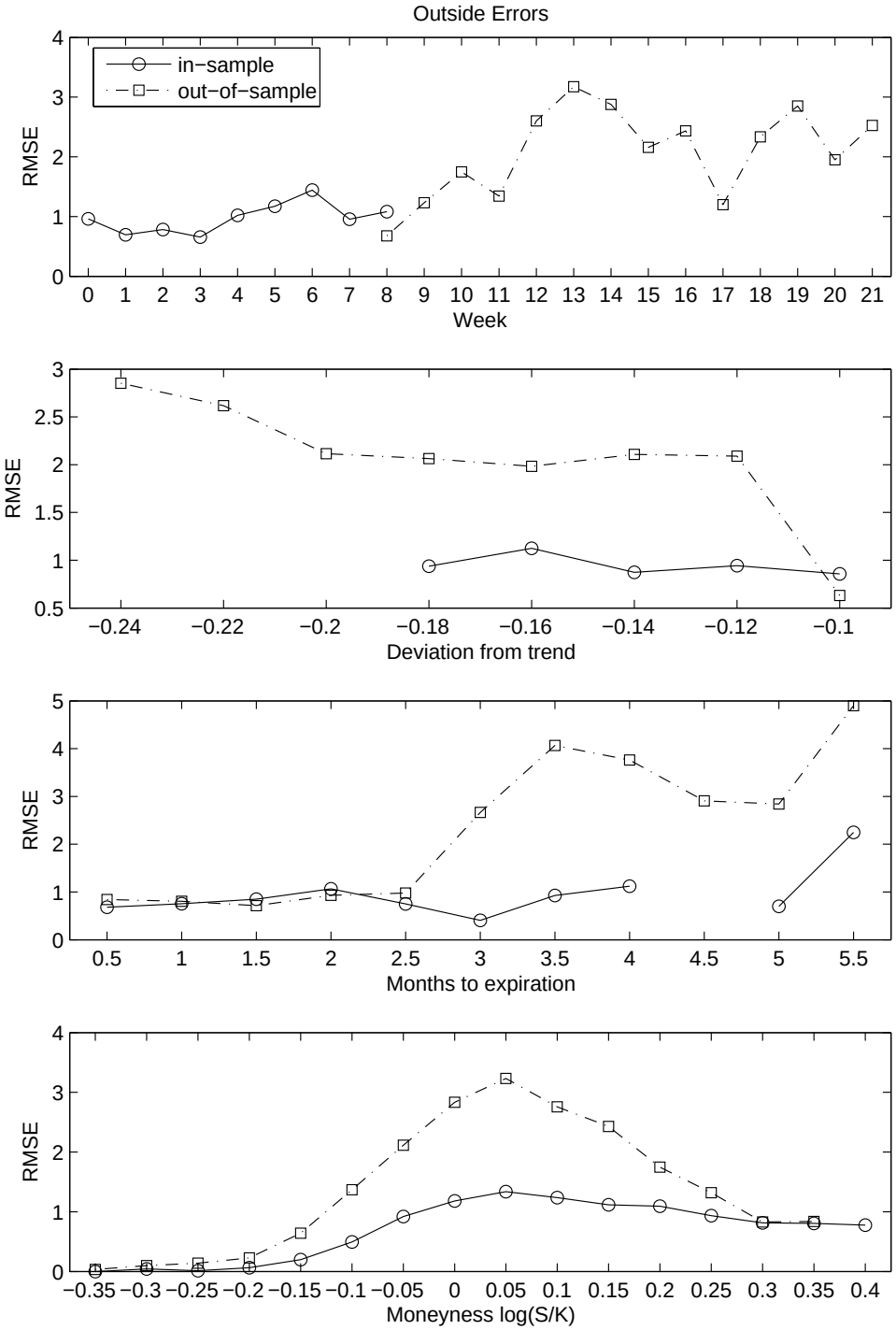

Figure 11: Plot of RMSEs versus observation time (measured in weeks), deviation from the mean, time to maturity (measured in months) and moneyness. In-sample (from January 17th to February 16th) and out-of-sample (from February 17th to May 23th) RMSEs are represented by circles and squares, respectively.